Product Specificity and Mechanism of Protein Lysine Methyltransferases: Insights from the Histone Lysine Methyltransferase SET8

Xiaodong Zhang and Thomas C. Bruice*

Department of Chemistry and Biochemistry, University of California, Santa Barbara, California 93106

Received February 11, 2008; Revised Manuscript Received April 30, 2008

ABSTRACT: Molecular dynamics simulations employing a molecular mechanics (MM) force field and hybrid quantum mechanics (QM) and MM (QM/MM) have been carried out to investigate the product specificity and mechanism of the histone H4 lysine 20 (H4-K20) methylation by human histone lysine methyltransferase SET8. At neutral pH, the target lysine is available to only the enzyme in the protonated state. The first step in the methylation reaction must be deprotonation of the lysine target which is followed by the $^+$AdoMet methylation of the neutral lysine [Enz•Lys-CH_2-NH_3^+•$^+$AdoMet → H^+ + Enz•Lys-CH_2-NH_2•$^+$AdoMet ⟶ Enz•Lys-CH_2-N(Me)H_2^+•AdoHcy]. The electrostatic interactions between two positive charges on $^+$AdoMet and Lys20-NH_3^+ decrease the pK_a of Lys20-NH_3^+. Upon formation of Enz•Lys-NH_3^+•$^+$AdoMet, a water channel by which the proton escapes to the outer solvent phase is formed. The formation of a water channel for the escape of a proton from Lys20-N(Me)H_2^+ in Enz•Lys20-N(Me)H_2^+•$^+$AdoMet is not formed because the methyl substituent blocks the starting of the water channel. Thus, a second methylation does not take place. The dependence of the occurrence of methyl transfer on the formation of a water channel in SET8 is in accord with our previous reports on product specificity by histone lysine monomethyltransferase SET7/9, large subunit lysine dimethyltransferase (LSMT), and viral histone lysine trimethyltransferase (vSET). The average value of the experimental $\Delta G_E^‡$ for the six lysine methyl transfer reactions catalyzed by vSET, LSMT, and SET7/9 with p53 as a substrate is 22.1 ± 1.0 kcal/mol, and the computed average ($\Delta G_C^‡$) is 22.2 ± 0.8 kcal/mol. In this study, the computed free energy barrier of the methyl transfer reaction [Lys20-NH_2 + $^+$AdoMet → Lys20-N(Me)H_2^+ + AdoHcy] catalyzed by SET8 is 20.8 kcal/mol. This is in agreement with the value of 20.6 kcal/mol calculated from the experimental rate constant (0.43 ± 0.02 min^{-1}). Our bond-order computations establish that the H4-K20 monomethylation in SET8 is a concerted linear S_N2 displacement reaction.

In eukaryotic cells, DNA is packaged in the format of chromatin. The chromatin is composed of the nucleosome which is built from the N-termini of four different histone enzymes. Post-translational modification, including the methylation at the site-specific target lysine, of these histone tails is vital in the adoption of a compacted chromatin structure (*1*).

All but one (*2, 3*) of the known protein lysine methyltransferases (PKMTs) (*4–16*) has a conserved domain, which is called the SET domain. PKMTs catalyze methyl transfer from *S*-adenosylmethionine ($^+$AdoMet) cofactor to the target lysine at the histone tails. Depending upon the PKMTs and lysine target, one, two, or three methyl transfers may occur. The number is called product specificity (Scheme 1).

We (*17–19*) have shown that each allowed methyl transfer step includes (i) the formation of a water channel which allows dissociation of the proton of target Lys-NH_3^+ and transfer to solvent, (ii) neutral lysine methylation by $^+$AdoMet, and (iii) release of AdoHcy and Enz•Lys-N(Me)H_2^+. Repeat of this sequence provides dimethylated lysine, and another repeat yields a trimethylated lysine. The formation of a water channel, or not, explains the processivity and multiplicity of the methyl transfer steps by PKMTs (Scheme 2).

Recently, the crystal structure of a member, SET8[1] (also known as Pre-SET7), of the PKMT family has been determined. Lysine H4-K20 can be methylated by a number of SET domain enzymes, including SET8, Suv4-20h1 (*20*), Suv4-20h2 (*20*), and NSD1 (*21*). Both Suv4-20h enzymes (*20*) are able to trimethylate H4-K20, while SET8 is highly selectively monomethylating H4-K20. We now report a molecular dynamics (MD) and hybrid SCCDFTB/MM methods [SCCDFTB (*29, 30*), self-consistent-charge density-functional tight-binding] study of the mechanism of H4-K20 methylation catalyzed by histone methyltransferase SET8.

MATERIALS AND METHODS

The initial structure of the SET8•Lys20•$^+$AdoMet complex was built from the X-ray structure [PDB entry 2BQZ (*10*)] of the SET8 enzyme with AdoHcy and the methylated Lys [Ly20-N(Me)] peptide substrate. In this X-ray structure [PDB entry 2BQZ (*10*)], water molecules are designated by

* To whom correspondence should be addressed. E-mail: tcbruice@chem.ucsb.edu. Telephone: (805) 893-2044. Fax: (805) 893-2229.

[1] Abbreviations: SET8, histone lysine methyltransferase; $^+$AdoMet, *S*-adenosylmethionine; AdoHcy, *S*-adenosyl-L-homocysteine; MD, molecular dynamics; SCCDFTB, self-consistent-charge density-functional tight-binding; CPR, conjugate peak refinement; TS, transition state.

10.1021/bi800244s CCC: $40.75
Published on Web 05/31/2008

Scheme 1

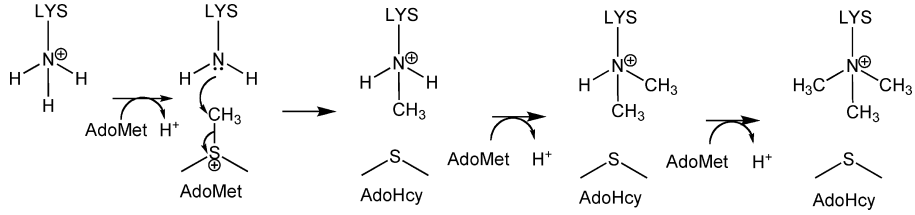

Scheme 2

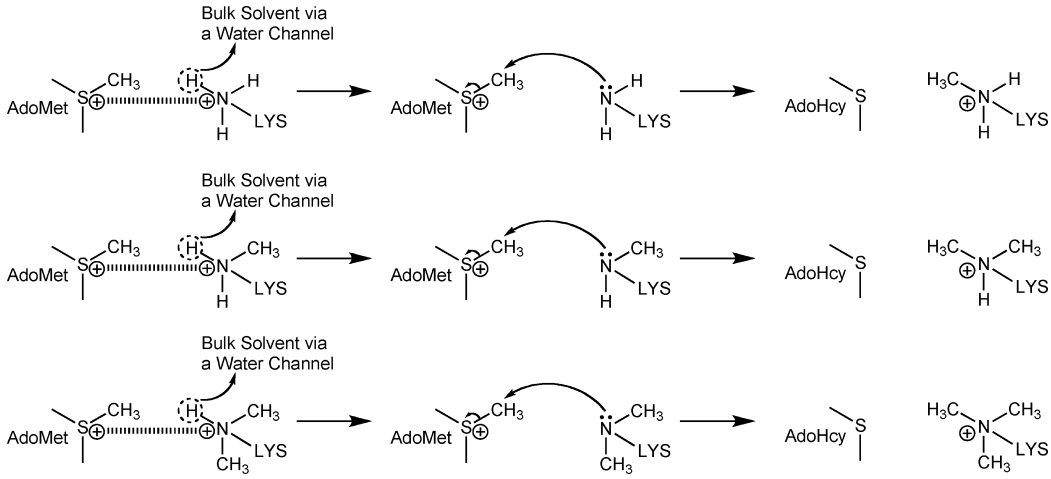

four fragments: U (1−17), V (1−247), Y (1−25), and Z (1−324). The methyl group of enzyme-bound $^+$AdoMet was built on the basis of the SET8•MeLys20•AdoHcy structure.

A water [TIP3P (*22*)] sphere with a 25 Å radius was centered at the $^+$AdoMet cofactor. Hydrogen atoms were added to the crystal structure using the HBUILD module implemented in CHARMM (*23*) (version 31b1), and CHARMM31-recognized all-atom 30-force field parameters (*24, 25*) were employed. A spherical boundary potential (*26*) for a 25 Å radius was used to prevent the water from "evaporating" from the surface. Each complex, including SET8•Lys20-NH_3^+, SET8•Lys20-NH_3^+•$^+$AdoMet, SET8•Lys20-NH_2•$^+$AdoMet, SET8•Lys20-N(Me)-H_2^+•AdoHcy, SET8•Lys20-N(Me)H_2^+, SET8•Lys20-N(Me)-H_2^+•$^+$AdoMet, and SET8•Lys20-N(Me)H•$^+$AdoMet, was minimized by the adopted basis Newton−Rasphon (ABNR) method until the gradient was less than 0.01 kcal mol^{-1} Å^{-1} at the MM level. Stochastic boundary molecular dynamics (SBMD) (*27*) were carried out for 3.0 ns on each complex. An integration time step of 1 fs was used, with all the bonds involving hydrogen atoms constrained using SHAKE (*28*).

The presence of a water channel is established by determining the distances between the hydrogen and oxygen atoms of the continuous water molecules. The average O···O distance in the water cluster has been determined to be 2.85 (*42*) and 2.94 Å (*43*) so that the O···H distance between the adjacent waters is <1.85 Å in the hydrogen bonds which form a water channel.

Fifteen snapshots of SET8•Lys20-NH_2•$^+$AdoMet and SET8•Lys20-N(Me)H•$^+$AdoMet complexes were picked at an interval of 200 ps from the 3 ns MD trajectories. Each of the 15 snapshots was minimized by SCCDFTB/MM methods [SCCDFTB (*29, 30*), self-consistent-charge density-functional tight-binding] until the gradient was less than 0.01 kcal mol^{-1} Å^{-1}, which led to an optimized structure of the reactant. The calculation of the SCCDFTB/MM term is described in refs *29* and *30* in detail. In the SCCDFTB/MM calculations, the SCCDFTB region included the -CH_2-S^+(Me)-CH_2- part of the $^+$AdoMet cofactor and the side chain of the neutral lysine 20 in the peptide substrate (Lys20-NH_2) [or neutral monomethylated lysine 20, Lys20-N(Me)H]. Link atoms were introduced to saturate the valence of the QM boundary atoms.

Adiabatic mapping calculations at the SCCDFTB/MM level were carried out using a two-dimensional potential energy surface (PES). The two-dimensional reaction coordinates were the N_ϵ(Lys20)−C_γ($^+$AdoMet) and C_γ($^+$AdoMet)−S_δ($^+$AdoMet) distances. The transition states were obtained by using conjugate peak refinement (CPR) (*31*) implemented in the Trajectory Refinement and Kinematics module of CHARMM, and normal-mode analysis provided only one imaginary frequency for characterizing the transition state. SCCDFTB for this methyl transfer reaction (*19*) is validated as compared with the B3LYP/6-31G*//MM calculations (*32*). The Wiberg bond-order analysis (*33*) of the bond making and breaking was carried out at the MP2/6-31+G(d,p)//MM level (Gamess-US version, June 22, 2002) (*34*) based on the transition state determined by SCCDFTB/MM.

The residues within 16 Å of $^+$AdoMet in all species (reactant, transition state, and product) were included in normal-mode analysis to provide $3N - 6$ frequencies, which were employed to calculate the zero-point energy, the thermal vibrational energy, and the entropy. (N is the number of atoms within the reduced regions; residues beyond that were fixed in the vibrational calculations.)

The free energies were obtained using the equation $\Delta G = \Delta E + \Delta E_{\mathrm{Ther}} + \Delta(\mathrm{ZPE}) - T\Delta S$ (*35*). To obtain more quantitative free energy barriers, single-point computations at the MP2/6-31+G(d,p)//MM (Gamess-US version, June 22, 2002) (*34*) level were carried out. The potential energy (ΔE)

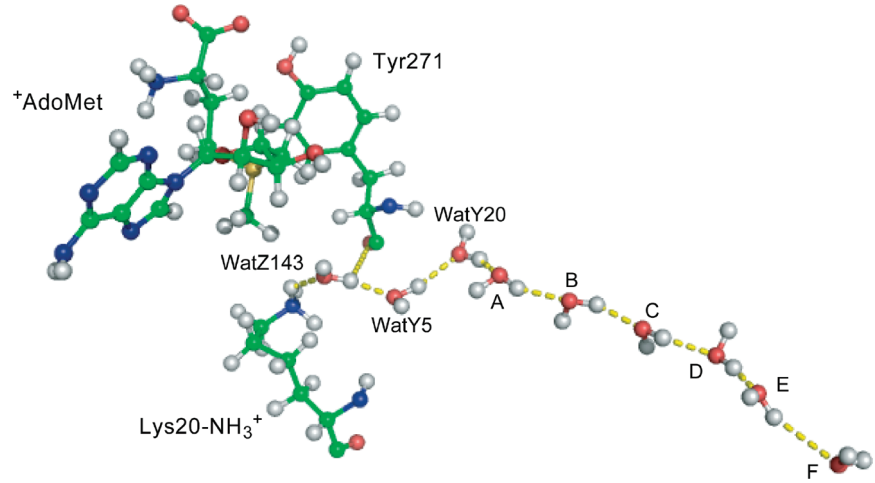

FIGURE 1: Snapshot of a water channel presenting 3 ns molecular dynamics simulations on species SET8·Lys20-NH_3^+·$^+$AdoMet.

Table 1: Average Densities (in atoms per cubic angstrom) of the Water Molecules at the Positions of a Water Channel (shown in Figure 1) during the MD Simulations on SET8·Lys20-NH_3^+·$^+$AdoMet[a]

	WatZ143	WatY5	WatY20	A	B	C	D	E	F
density	0.006	0.008	0.009	0.013	0.018	0.022	0.023	0.023	0.018

[a] The solvent water molecules are designated by A−F, and F is on the surface of the water sphere with a 25 Å radius. The crystal water molecules are designated by Wat.

was provided by QM/MM. The thermal energy (ΔE_{Ther}) could be expressed as $\Delta E_{Ther} = \Delta E_{Trans} + \Delta E_{Rot} + \Delta E_{Vib}$. The vibrational contributions [Δ(ZPE), ΔE_{Vib}, and $-T\Delta S$] were determined with harmonic approximation at 298 K by normal-mode analysis. Because the thermal energies and entropies from the transition motion (E_{Trans}) and rotation motion (E_{Rot}) are linear with temperature according to their corresponding statistical equations, their contributions to the reaction barrier (or reaction energy) should be approximately zero for an enzymatic reaction at a constant temperature. From comparison of the computational and experimental free energy of activation (see Conclusions), umbrella sampling or potential of mean force would have no advantage. Thus, the equation $\Delta G = \Delta E + \Delta E_{vib} + \Delta$(ZPE) $- T\Delta S$ is used in this study.

RESULTS AND DISCUSSION

The Neutral Lys20-NH_2 Peptide Substrate Is Created at the Time of Formation of a Water Channel. Throughout 3 ns trajectories of MD simulations on the SET8·Lys20-NH_3^+·$^+$AdoMet complex, a water channel, associated with a statistical 66.7% presence based on the distance (<1.85 Å), allows dissociation of a proton of Lys20-NH_3^+ into the solvent (Figure 1). Our previous reports (*17–19, 41*) of 3 ns MD simulations on each complex [Enz·Lys-NH_3^+, Enz·Lys-NH_3^+·$^+$AdoMet, Enz·Lys-N(Me)H_2^+, Enz·Lys-N(Me)H_2^+·$^+$AdoMet, Enz·Lys-N(Me)$_2$$H^+$, and Enz·Lys-N(Me)$_2$$H^+$·$^+$AdoMet] indicate that these structures are very stable. The electrostatic interaction between two positive charges on the cofactor and (methylated) substrate decreases the pK_a of the (methylated) substrate. Only a water channel appears in SET7/9·Lys4-NH_3^+·$^+$AdoMet, LSMT·Lys-NH_3^+·$^+$AdoMet, LSMT·Lys-N(Me)H_2^+·$^+$AdoMet, vSET·Lys27-NH_3^+·$^+$AdoMet, vSET·Lys27-N(Me)H_2^+·$^+$AdoMet, and vSET·Lys27-N(Me)$_2$$H^+$·$^+$AdoMet. These findings afford a definitive explanation to product specificity by PKMTs (Scheme 2). Methyl transfer does not occur if a water channel is not present. Each allowed methyl transfer step includes (i) the formation of a water channel to allow dissociation of a proton from protonated charged lysine into solvent, (ii) methylation of a neutral lysine by $^+$AdoMet, and (iii) product formation and release. The formation of a water channel, or not, explains the processivity and multiplicity of the methyl transfer steps by PKMTs. Much longer MD simulations should provide the same evidence that the ability or inability to form a water channel determines whether methyl transfer occurs.

The average densities (Table 1) and the O···H distance of <1.85 Å between the adjacent water confirm the formation of a water channel.

An enzyme-bound water (WatZ143) is hydrogen bonded to Lys20-NH_3^+ and becomes the starting point of the water channel (Figure 1). Examination of the environment around the water channel shows that there is no base present that can assist proton departure. When a hydroxide ion (HO^-) is positioned at A (Figure 1), there should be no energy barrier for the proton dissociation of Lys20-NH_3^+ because the pK_a of HOH (~16.0) is much greater than that of Lys-N^+H_2H (~10.0). Both SCCDFTB/MM and HF/6-31+G(d,p)//MM computations confirm that there is no energy barrier for proton transfer from Lys20-NH_3^+ to HO^- positioned at A (Figure 1). Because the concentration of HO^- at an optimal pH of 8.0 is 10^{-6}, the observed energy barrier for proton dissociation would be 8.4 kcal/mol.

Mechanism for the First Methyl Transfer Step. The reaction coordinates for the first methyl transfer reaction [SET8·Lys20-NH_2·$^+$AdoMet → SET8·Lys20-N(Me)H_2^+·AdoHcy] are depicted in Figure 2. The key geometric parameters of the ground, transition, and product states as well as the bond order at the transition state are also given in Figure 2.

Normal-mode analysis characterizes the transition state (TS-M) of the first methylation step with only one imaginary frequency of 399 ± 94i cm^{-1}. The linear S_δ($^+$AdoMet)···C_γ

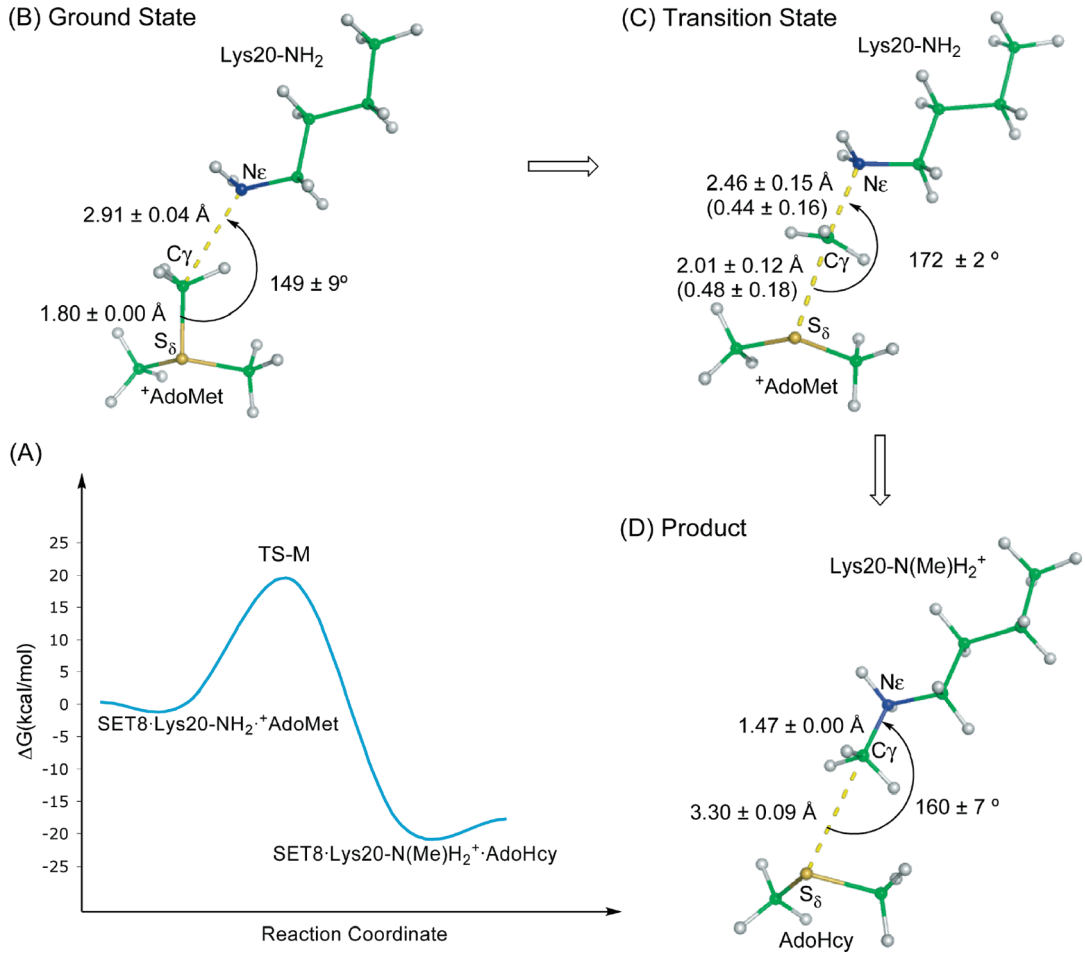

FIGURE 2: (A) Schematic free energy profile for the methyl transfer reaction by SET8. The key geometric parameters of (B) ground-state SET8•Lys20-NH_2•$^+$AdoMet, (C) transition state TS-M, and (D) product state SET8•Lys20-N(Me)H_2^+•AdoHcy are given. The numbers in parentheses are the bond orders at TS-M.

($^+$AdoMet)•••N_ϵ(Lys20-NH_2) configuration (Figure 2C) of the TS-M as well as the bond-order analysis (Figure 2C) of N_ϵ(Lys20-NH_2)•••C_γ($^+$AdoMet) and C_γ($^+$AdoMet)•••S_δ-($^+$AdoMet) bonds of the TS-M is characterized as a concerted S_N2 displacement (*36*). These features are shared by the transition states of the first methyl transfer step catalyzed by SET7/9, LSMT, and vSET (*17–19, 41*).

The calculated average free energy barrier of the methyl transfer reaction is as follows: $\Delta G_C^{\ddagger} = \Delta E_C^{\ddagger} + \Delta(ZPE)_C^{\ddagger} - T\Delta S_C^{\ddagger} + \Delta E_{Vib,C}^{\ddagger} = 13.7 - 0.2 + 0.8 - 0.4 = 13.9$ kcal/mol. The deviations of $\Delta G_C^{\ddagger}$, $\Delta E_C^{\ddagger}$, $\Delta(ZPE)_C^{\ddagger}$, $T\Delta S_C^{\ddagger}$, and $\Delta E_{Vib,C}^{\ddagger}$ are ±2.3, ±2.5, ±0.5, ±0.8, and ±0.2 kcal/mol, respectively. Because the frequency of the formation of a water channel in the SET8•Lys20-NH_3^+•$^+$AdoMet complex is 66.7%, the observed free energy barrier ($\Delta G_{obs}^{\ddagger}$) equals $\Delta G_C^{\ddagger}$/66.7% = 20.8 kcal/mol (Figure 2A), which is in agreement with the free energy barrier (20.6 kcal/mol) calculated from the experimental rate constant (0.43 ± 0.02 min^{-1}) (*9*). Thus, the result presented here could not likely be improved by employing the more rigorous, but time-consuming, umbrella sampling method.

The enzyme-catalyzed methyl transfer reaction is calculated to be exergonic overall: $\Delta G_C^{\circ} = \Delta E_C^{\circ} + \Delta(ZPE)_C^{\circ} - T\Delta S_C^{\circ} + \Delta E_{Vib,C}^{\circ} = -17.1 + 2.8 - 0.6 - 0.1 = -15.0$ kcal/mol (Figure 2A). The deviation in ΔG_C° is ±5.6 kcal/mol.

Product Specificity of SET8. The water channel, so important in enzyme activity, is not present in either the product SET8•Lys20-N(Me)H_2^+•AdoHcy or SET8•Lys20-N(Me)H_2^+. More importantly, formation of the SET8•Lys20-N(Me)H_2^+•$^+$AdoMet complex is not followed by dissociation of a proton from Lys20-N(Me)H_2^+ because the methyl substituent blocks the formation of a water channel by being in the position that Lys-H must occupy (Figure 3). Mutation Tyr245Phe in SET7/9 has been reported to convert the enzyme from a mono- to a dimethyltransferase (*44*). We have found by MD simulation that this mutated SET7/9[Y245F]•Lys4-N(Me)H_2^+•$^+$AdoMet complex has a water channel (*18*). Thus, a future goal is to find what mutation, in particular Tyr245, would have significant influences on the activation barrier and product specificity of SET8.

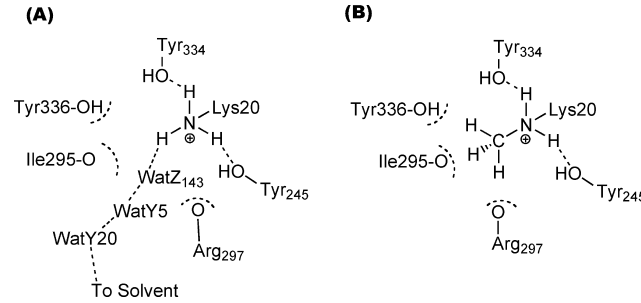

FIGURE 3: Schematic diagram of the position of the amine group at (A) SET8•Lys20-NH_3^+•$^+$AdoMet and (B) SET8•Lys20-N(Me)H_2^+•$^+$AdoMet.

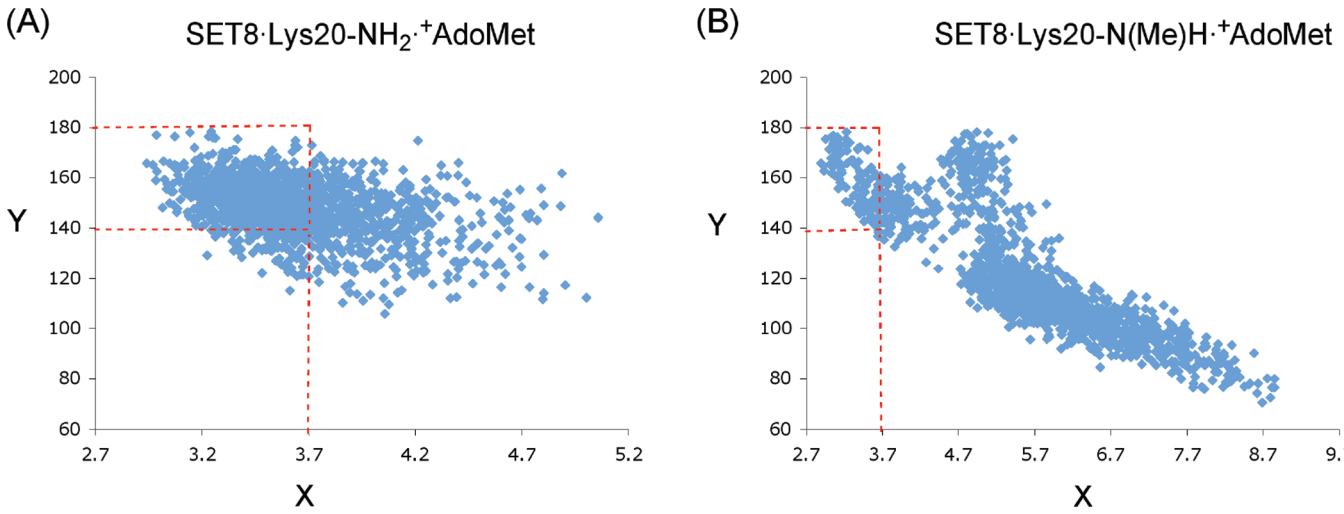

FIGURE 4: Distributions of configurations at the (A) SET8·Lys20-NH_2·$^+$AdoMet and (B) SET8·Lys20-N(Me)H·$^+$AdoMet ground states. The Cγ($^+$AdoMet)···Nϵ(Lys20-NH_2) {or Cγ($^+$AdoMet)···N[Lys20-N(Me)H]} bond length is on the *x*-axis and in angstroms, and the Sδ($^+$AdoMet)−Cγ($^+$AdoMet)···N(Lys20-NH_2) {or Sδ($^+$AdoMet)−Cγ($^+$AdoMet)···N[Lys20-N(Me)H]} bond angle is on the *y*-axis and in degrees. For NACs, we allow 160 ± 20° for the bond angle (*y*-axis) and ≤3.7 Å for the bond length (*x*-axis).

Also, the fact that methyl transfer is dependent upon the presence of a water channel is in excellent agreement with our previous studies (*17–19, 41*) of the LSMT (dimethyltransferase with a single lysine as a substrate), vSET (trimethyltransferase), and SET7/9 (monomethyltransferase) enzymes. Thus, the formation of a water channel determines whether methyl transfer reactions catalyzed by all SET domain enzymes occur (Scheme 2).

NAC Contributions to the Product Specificity. If we suppose that the Lys20-N(Me)H_2^+ proton dissociation provides SET8·Lys20-N(Me)H·$^+$AdoMet, the configurations at the ground states would be as shown in Figure 4.

For a reaction to take place, the reacting atoms must come together to van der Waals separation and at angles resembling that in the transition state. Such near-attack conformations (NACs) are the doors through which the ground state must pass to the transition state (*38–40*). For NACs, we allow 160 ± 20° for the bond angle (*y*-axis in Figure 4) and ≤3.7 Å for the bond length (*x*-axis in Figure 4). Thus, SET8·Lys20-NH_2·$^+$AdoMet has 952 NACs, while SET8·Lys20-N(Me)H·$^+$AdoMet has 97 NACs (Figure 4). This provides additional evidence for SET8 as a monomethyltransferase to catalyze the H4-K20 peptide substrate.

Supposed "Second" Methyl Transfer Reaction Step. By single-point MP2/6-31+G(d,p)//MM, the calculated average free energy barrier for the second methyl transfer step is $\Delta G_C^{\ddagger} = \Delta E_C^{\ddagger} + \Delta(\mathrm{ZPE})_C^{\ddagger} - T\Delta S_C^{\ddagger} + \Delta E_{\mathrm{Vib,C}}^{\ddagger} = 34.7 + 0.9 + 2.2 - 0.7 = 37.1$ kcal/mol. The deviations of $\Delta G^{\ddagger}$, $\Delta E^{\ddagger}$, $\Delta(\mathrm{ZPE})^{\ddagger}$, $T\Delta S^{\ddagger}$, and $\Delta E_{\mathrm{Vib}}^{\ddagger}$ are ±6.2, ±4.8, ±0.7, ±1.6, and ±0.5 kcal/mol, respectively. As compared with the average free energy barrier (20.8 kcal/mol) for the allowed methyl transfer step, this higher free energy barrier of 37.1 kcal/mol for the forbidden reaction [Lys20-N(Me)H + $^+$AdoMet → Lys20-N$(Me)_2H^+$ + AdoHcy] suggests that the higher energy barrier from NAC at the SET8·Lys20-N(Me)H·$^+$AdoMet ground state is what makes the reaction unfavorable.

Normal-mode analysis shows that the transition state (TS-D) of the supposed second step [SET8·Lys20-N(Me)H·$^+$AdoMet → SET8·Lys20-N$(Me)_2H^+$·AdoHcy] has one and only one imaginary frequency of 303 ± 122i cm^{-1}. In the TS-D, the N[Lys20-N(Me)H]···Cγ($^+$AdoMet) and Cγ($^+$AdoMet)···Sδ($^+$AdoMet) bond lengths are 2.46 ± 0.12 and 2.14 ± 0.14 Å, respectively, and the N[Lys20-N(Me)H]···Cγ($^+$AdoMet)···Sδ($^+$AdoMet) bond angle is 157 ± 14°. This nonlinear bond angle is not favorable for a S_N2 reaction and indicates an alternative factor for the product specificity of SET8.

CONCLUSIONS

We have now employed the histone H4 lysine 20 (H4-K20) methylation by SET8 in the study of the product specificity of protein lysine methyltransferases. MD simulations show that a water channel appears only in the SET8·Lys20-NH_3^+·$^+$AdoMet complex. The electrostatic interactions between two positive charges on $^+$AdoMet and Lys20-NH_3^+ decrease the pK_a of Lys20-NH_3^+. The dissociation of the proton of Lys20-NH_3^+ occurs, which is associated with a barrier of 8.4 kcal/mol at pH 8.0, via this water channel. A water channel does not form in SET8·Lys20-N$(Me)H_2^+$·AdoHcy, SET8·Lys20-NH_3^+, or SET8·Lys20-N$(Me)H_2^+$. Notably, a water channel does not appear in the SET8·Lys20-N$(Me)H_2^+$·$^+$AdoMet complex. The conformation of the nitrogen substituent of Lys20-CH_2N$(Me)H_2^+$ (Figure 3) determines the presence, or absence, of the water channel and proton dissociation that creates the neutral Lys20-N(Me)H substrate. Also, noting the dependence of methyl transfer occurring on the formation of a water channel in our previous studies of SET7/9, LSMT, and vSET (*17–19*) establishes a definitive mechanism (Scheme 2). Also, the comparison (Figure 4) of the near-attack conformations of the ground states SET8·Lys20-NH_2·$^+$AdoMet and SET8·Lys20-N(Me)H·$^+$AdoMet as well as the configuration at the transition states (172 ± 2° in Figure 2 and 157 ± 14° in the text) for the two reactions provides additional information for the product specificity of SET8. Our calculated free energy barrier, $\Delta G_C^{\ddagger}$, for the methyl transfer reaction [SET8·Lys20-NH_2·$^+$AdoMet → SET8·Lys20-N$(Me)H_2^+$·AdoHcy] is 13.9 ± 2.3 kcal/mol. The presence of water channel is 66.7% likely, so the observed free energy barrier ($\Delta G_{\mathrm{obs}}^{\ddagger}$) equals $\Delta G_C^{\ddagger}/0.667 = 13.9/0.667 = 20.8$ kcal/mol, which is in excellent agreement with the free energy barriers

of 20.6 kcal/mol calculated from the experimental rate constants (0.43 ± 0.02 min^{-1}) (*9*). The worth of any computational method for determining the reaction coordinates for an enzymatic reaction can be judged by comparing the computed free energy of reaction ($\Delta G_C^{\ddagger}$) to the experimental $\Delta G_E^{\ddagger}$ determined from k_{cat}. The average value of the experimental $\Delta G_E^{\ddagger}$ for the six lysine methyl transfer reactions carried out by vSET (*19*), LSMT (*17*), and SET7/9 (*41*) with p53 as a substrate is 22.1 ± 1.0 kcal/mol, and the computed average $\Delta G_C^{\ddagger}$ equals 22.2 ± 0.8 kcal/mol. In this study, $\Delta G_E^{\ddagger} = 20.6$ kcal/mol and $\Delta G_C^{\ddagger} = 20.8$ kcal/mol. Thus, these results could not be made better by employing the more rigid, but time-consuming, umbrella sampling or potential of mean force method.

ACKNOWLEDGMENT

Some of the calculations were performed at the National Center for Supercomputing Applications (University of Illinois, Urbana, IL).

REFERENCES

1. Strahl, B. D., and Allis, C. D. (2000) The language of covalent histone modifications. *Nature 403*, 41–45.
2. Feng, Q., Wang, H., Ng, H. H., Erdjument-Bromage, H., Tempst, P., Struhl, K., and Zhang, Y. (2002) Methylation of H3-lysine 79 is mediated by a new family of HMTases without a SET domain. *Curr. Biol. 12*, 1052–1058.
3. Min, J., Feng, Q., Li, Z. Z., Zhang, Y., and Xu, R. M. (2003) Structure of the catalytic domain of human DOT1L: A non-SET domain nucleosomal histone methyltransferase. *Cell 112*, 711–723.
4. Jacobs, S. A., Harp, J. M., Devarakonda, S., Kim, Y., Rastinejad, F., and Khorasanizadeh, S. (2002) The active site of the SET domain is constructed on a knot. *Nat. Struct. Biol. 9*, 833–838.
5. Xiao, B., Jing, C., Wilson, J. R., and Gamblin, S. J. (2003) SET Domain and Histone Metylation. *Curr. Opin. Struct. Biol. 13*, 699–705.
6. Xiao, B., Jing, C., Wilson, J. R., Walker, P. A., Vasisht, N., Kelly, G., Howell, S., Taylor, I. A., Blackburn, G. M., and Gamblin, S. J. (2003) Structure and Catalytic Mechanism of the Human Histone Methyltransferase SET 7/9. *Nature 421*, 652–656.
7. Kwon, T., Chang, J. H., Kwak, E., Lee, C. W., Joachimiak, A., Kim, Y. C., Lee, J., and Cho, Y. (2002) Mechanism of histone lysine methyl transfer revealed by the structure of SET7/9-AdoMet. *EMBO J. 22*, 292–303.
8. Couture, J., Collazo, E., Hauk, G., and Trievel, R. C. (2006) Structural Basis for the Methylation Site Specificity of SET7/9. *Nat. Struct. Mol. 13*, 140–146.
9. Couture, J., Collazo, E., Brunzelle, J. S., and Trievel, R. C. (2005) Structural and functional analysis of SET8, a histone H4 Lys-20 methyltransferase. *Genes Dev. 19*, 1455–1465.
10. Xiao, B., Jing, C., Kelly, G., Walker, P. A., Muskett, F. W., Frenkiel, T. A., Martin, S. R., Sarma, K., Reinberg, D., Gamblin, S. J., and Wilson, J. R. (2005) Specificity and mechanism of the histone methyltransferase Pr-Set7. *Genes Dev. 19*, 1444–1454.
11. Zhang, X., Yang, Z., Khan, S. I., Horton, J. R., Tamarn, H., Selker, E. U., and Cheng, X. (2003) Structural basis for the product specificity of histone lysine methyltransferase. *Mol. Cell 12*, 177–185.
12. Min, J., Zhang, X., Cheng, X., Grewal, S. I., and Xu, R. M. (2002) Structure of the SET domain histone lysine methyltransferase Clr4. *Nat. Struct. Biol. 9*, 828–832.
13. Qian, C., Wang, X., Manzur, K., Farooq, S. A., Zeng, L., Wang, R., and Zhou, M. (2006) Structural Insights of the Specificity and Catalysis of a Viral Histone H3 Lysine 27 Methyltransferase. *J. Mol. Biol. 359*, 86–96.
14. Manzur, K. L., Farooq, A., Zeng, L., Plotnikova, O., Koch, A. W., Sachchildanand, and Zhou, M. M. (2003) A dimeric viral SET domain methyltransferase specific to Lys27 of histone H3. *Nat. Struct. Biol. 10*, 187–196.
15. Trivel, R. C., Flynn, E. M., Houtz, R. L., and Hurley, J. H. (2003) Mechanism of Multiple Lysine Methylation by the SET Domain Enzyme Rubisco LSMT. *Nat. Struct. Biol. 10*, 545–552.
16. Couture, J., Hauk, G., Thompson, M. J., Blackburn, G. M., and Trievel, R. C. (2006) Catalytic Roles for Carbon-Oxygen Hydrogen Bonding in SET Domain Lysine Methyltransferases. *J. Biol. Chem. 281*, 19280–19287.
17. Zhang, X. D., and Bruice, T. C. (2007) Catalytic Mechanism and Product Specificity of Rubisco Large Subunit Methyltransferase: QM/MM and MD Investigations. *Biochemistry 46*, 5505–5014.
18. Zhang, X.-D., and Bruice, T. C. (2007) Histone Lysine Methyltransferase SET7/9: Formation of a Water Channel Precedes Each Methyl Transfer. *Biochemistry 46*, 14838–14844.
19. Zhang, X.-D., and Bruice, T. C. (2007) A QM/MM Study on the Catalytic Mechanism and Product Specificity of viral Histone Lysine Methyltransferase. *Biochemistry 46*, 9743–9751.
20. Schotta, G., Lachner, M., Sarma, K., Ebert, A., Sengupta, R., Reuter, G., Reinberg, D., and Jenuwein, T. (2004) A silencing pathway to induce H3-K9 and H4-K20 trimethylation at constitute heterochromatin. *Genes Dev. 18*, 1251–1262.
21. Rayasam, G. V., Wendling, O., Angrand, P. O., Mark, M., Niederreither, K., Song, L., Lerouge, T., Hager, G. L., Chambon, P., and Losson, R. (2003) NSD1 is essential for early post-implantation development and has a catalytically active SET domain. *EMBO J. 22*, 3153–3168.
22. Jorgensen, W. L., Chandrasekhar, J., Madura, J. D., Impey, R. W., and Klein, K. L. (1983) Comparison of simple potential functions for simulating liquid water. *J. Chem. Phys. 79*, 926–935.
23. Brooks, B. R., Bruccoleri, R. E., Olafson, B. D., States, D. J., Swaminathan, S., and Karplus, M. (1983) CHARMM: A Program for Macromolecular Energy, Minimization, and Dynamics Calculations. *J. Comput. Chem. 4*, 187–217.
24. MacKerell, A. D., Feig, M., and Brooks, C. L. (2004) Extending the treatment of backbone energetics in protein force fields: Limitations of gas-phase quantum mechanics in reproducing protein conformational distributions in molecular dynamics simulations. *J. Comput. Chem. 25*, 1400–1415.
25. MacKerell, A. D., Jr., Bashford, D., Bellott, M., Dunbrack, R. L., Evanseck, J. D., Field, M. J., Fischer, S., Gao, J., Guo, H., Ha, S., Joseph-McCarthy, D., Kuchnir, L., Kuczera, K., Lau, F. T. K., Mattos, C., Michnick, S., Ngo, T., Nguyen, D. T., Prodhom, B., Reiher, W. E., Roux, B., Schlenkrich, M., Smith, J. C., Stote, R., Straub, J., Watanabe, M., Wiorkiewicz-Kuczera, J., Yin, D., and Karplus, M. (1998) All-Atom Empirical Potential for Molecular Modeling and Dynamics Studies of Proteins. *J. Phys. Chem. B 102*, 3586–3616.
26. Brunger, A. T., Brooks, C. L., III, and Karplus, M. (1985) Active Site Dynamics of Ribonuclease. *Proc. Natl. Acad. Sci. U.S.A. 82*, 8458–8462.
27. Brooks, C. L., and Karplus, M. (1989) Solvent Effects on Protein Motion and Protein Effects on Solvent Motion: Dynamics of the Active Site Region of Lysozyme. *J. Mol. Biol. 208*, 159–181.
28. Ryckaert, J. P., Ciccotti, G., and Berendsen, H. J. C. (1977) Numerical integration of the cartesian equations of motion of a system with constraints: Molecular dynamics of n-alkanes. *J. Comput. Phys. 23*, 327–341.
29. Cui, Q., Elstner, M., Kaxiras, E., Frauesheim, Th., and Karplus, M. (2001) A QM/MM Implementation of the Self-Consistent Charge Density Functional Tight Binding (SCC-DFTB) Method. *J. Phys. Chem. B 105*, 569–585.
30. Elstner, M., Porezag, D., Jungnickel, G., Elsner, J., Haugk, M., Frauenheim, Th., Suhai, S., and Seifert, G. (1998) Self-Consistent-Charge Density-Functional Tight-Binding Method for Simulation of Complex Materials Properties. *Phys. Rev. B 58*, 7260–7268.
31. Fischer, S., and Karplus, M. (1992) Conjugate Peak Refinement: An Algorithm for Finding Reaction Paths and Accurate Transition States in Systems with Many Degrees of Freedom. *Chem. Phys. Lett. 194*, 252–261.
32. Hu, P., and Zhang, Y. (2006) Catalytic Mechanism and Product Specificity of the Histone Lysine Methyltransferase SET 7/9: An ab initio QM/MM-FE study with Multiple Initial Structures. *J. Am. Chem. Soc. 128*, 1272–1278.
33. Wiberg, K. B. (1968) Application of the Pople-Santry-Segal complete neglect of differential overlap method to the cyclopropylcarbinyl and cyclobutyl cation and to bicyclobutane. *Tetrahedron 24*, 1083–1096.
34. Schmidt, M. W., Baldridge, K. K., Boatz, J. A., Elbert, S. T., Gorden, M. S., Jensen, J. H., Koseki, S., Matsunage, N., Nguyen, K. A., Su, S. J., Windus, T. L., Dupuis, M., and Montgomery, J. A. (1993) General atomic and molecular electronic-structure system. *J. Comput. Chem. 14*, 1347–1363.

35. McQuarrie, D. A. (1973) *Statistical Thermodynamics*, Harper and Row, New York.
36. Takusagawa, F., Fujioba, M., Spies, A., and Schowen, R. L. (1998) S-Adenosylmethionine (AdoMet)-dependent Methyltransferases, in *Comprehensive Biological Catalysis: A Mechanistic Reference* (Sinnott, M., Ed.) pp 1−30, Academic Press, New York.
37. Wang, S., Hu, P., and Zhang, Y. (2007) Ab Initio Quantum mechanical/Molecular Mechanism Molecular Dynamics Simulations of Enzyme Catalysis: The Case of Histone Lysine Methyltransferase SET7/9. *J. Phys. Chem. B 111*, 3758–3764.
38. Bruice, T. C. (2002) A view at the millennium: The efficiency of enzyme catalysis. *Acc. Chem. Res. 35*, 139–148.
39. Bruice, T. C., and Benhovic, S. J. (2000) Chemical basis for enzyme catalysis. *Biochemistry 39*, 6267–6274.
40. Bruice, T. C. (2006) Computational approaches: Reaction trajectories, structures, and atomic motions. Enzyme reactions and proficiency. *Chem. Rev. 106*, 3119–3139.
41. Zhang, X.-D., and Bruice, T. C. (2008) Mechanism of product specificity of AdoMet methylation catalyzed by lysine methyltransferases: Transcriptional factor p53 methylation by histone lysine methyltransferase SET7/9. *Biochemistry 47*, 2743–2748.
42. Lu, J., Yu, J., Chen, X., Cheng, P., Zhang, X., and Xu, J. (2005) Novel Self-Assembled Chain of Water Molecules in a Metal-Organic Framework Structure of Co(II) with Tartrate Acid. *Inorg. Chem. 44*, 5978–5980.
43. Jin, Y., Che, Y., and Zheng, J. (2007) Supramolecularly assembled decameric water cluster stabilized by dichromate anions in complex of Ni(II). *Inorg. Chem. Commun. 10*, 514–516.
44. Cheng, X., Collins, R., and Zhang, X. (2005) Structural and Sequence Motifs of Protein (Histone) Methylation Enzymes. *Annu. Rev. Biophys. Biomol. Struct. 34*, 267–294.

BI800244S